CRUSTAL STRENGTH VARIATIONS ON CERES AS REVEALED BY ITS IMPACT CRATERS. M. F. Zeilnhofer and N. G. Barlow, Dept. Astronomy & Planetary Science, Northern Arizona University, Flagstaff, AZ 86011-6010 mfz3@nau.edu, Nadine.Barlow@nau.edu

Introduction: Ceres is the largest body in the main asteroid belt with a mean radius of ≈ 473 km and a density of 2162 kg/m^3 [1]. Due to Ceres' low-density, pre-Dawn proposals suggested viscous relaxation would occur erasing the impact craters on the surface [2]. Instead the Dawn spacecraft attained images of a heavily cratered surface [3].

We have conducted a study of to identify global distributions of impact crater morphologies and morphometries as well as regional distributions to identify crustal difference across Ceres. The crater morphologies include central peaks and central pits which have been related to near-surface characteristics including target strength and volatile content [4-5]. The peak-to-crater diameter ratio (D_{pk}/D_c) increases as target strength decreases and the pit-to-crater diameter (D_p/D_c) ratio decreases with an increase in gravity and a decrease in volatile content [4].

Three types of lobate flow features are classified on Ceres relating to landslide-type flows seen on Earth and Mars (type 1), flow material deposited on the crater floor similar to what is found on Iapetus (type 2), and deposits similar to layered ejecta blankets found on Mars and Ganymede (type 3) [6]. Classifying these flow features on Ceres help identify areas which are weak enough to allow material to flow and thus provide further insight into the crustal properties of Ceres.

Polygonal craters are also of interest due to their widespread presence across the surface of Ceres indicating a weakened crust due to the presence of fracture systems within the surface and subsurface [7-11]. Polygonal craters are found on rocky and icy bodies and for rocky bodies are generally 10-20% of all known craters [8].

Methodology: We have complied a near-global crater database for Ceres containing 44,594 craters ≥ 1.0 km in diameter [12]. Data were attained from the Framing Camera (FC) onboard the Dawn spacecraft with a resolution of 400 m/pixel. The crater interior morphologies and crater morphometries were analyzed using the Low Altitude Mapping Orbit (LAMO) data with a resolution of 35 m/pixel [13]. Central peak, central pit, lobate flow features and polygonal crater length measurements were measured within the Java Mission-planning and Analysis for Remote Sensing (JMARS) [14] while the crater depths were measured using the topography models found within JMARS (oblate and mean sphere) and the polygonal crater angle measurements were measured using ImageJ, an image processing tool.

Craters with floor deposits were placed into a separate database to record the type of floor deposits (type 1-3). Additionally, there were two other types of lobate flow features added to the analysis: craters which have a combination of type 2 and type 3 lobate flow features, and features which were similar to type 2 features (generic floor deposits) but could not fully be distinguished as type 2, most likely due to resolution.

The polygonal craters (PC) were also placed into a separate database for more thorough analysis. The PC database contains 1,466 craters with four categories: PC with no relation to visible fractures, PC related to visible fracture systems located outside of the crater, PC with fractures located inside of the crater and PC with fractures located inside and outside of the crater [10]. To determine if a PC was related to a fracture system outside of the crater, we used a maximum bound of 10 crater radii from the crater's center. The polygonal crater database also includes the number of linear rim segments (4-12), the angle between the sides and the mean angle for the crater, the length of the linear rim segments and the mean length for the crater and the crater and the angle of the linear rim segment with relation to the fracture systems with the mean angle for the crater [10,16]. These fracture systems were previously mapped and include the catenae systems of Samhain, Uhola, Pongal, Baltay, Gerner, and Junina [15]. Fractures found within a crater were reported as floor fractured craters (FFCs) in the global crater database.

Preliminary Results: Analysis of the distribution of interior morphologies and crater morphometries shows interesting variations between the northern and southern hemispheres. Central peaks are distributed across the entire surface while central floor pits are concentrated from 10.55º-74.05ºN and summit pits occur evenly between the two hemispheres.

The median D_{pk}/D_c becomes larger in the northern hemisphere, with the larger values beginning at 40ºN [Figure 1]. The median D_p/D_c also becomes larger near the north pole indicating the northern hemisphere crust is weaker than that in the southern hemisphere. This could be due to a more

fractured/brecciated crust and/or higher volatile content in the north. The depth-diameter (d/D) ratio for craters with wall terraces is larger between 50-70ºN, latitude indicating these craters are excavating deeper into the subsurface for the same amount of impact energy, which also suggests a weaker target material.

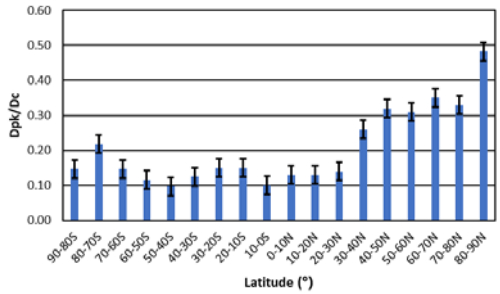

Figure 1: The median D_{pk}/D_c reported for each 10° latitude zone in which central peaks were identified. Standard error bars were calculated.

The lobate flow features also show variations with latitude [Figure 2]. The type 1 lobate flow features are found in the upper mid-latitudes and the polar regions with a higher frequency at the south pole when normalized to area. Type 2 lobate flow features are most frequent in the mid-latitude regions whereas the generic floor deposits are concentrated in the mid-latitude regions in the southern hemisphere. Type 3 lobate flow features are concentrated in the mid- latitude regions in the southern hemisphere and the combination type 2 and type 3 are typically found in the higher northern latitudes.

Polygonal craters comprise ~3.3% of all impact craters on Ceres and were highly concentrated north of 60º [Figure 3] even though they are distributed across the entire surface [10,16]. A majority of the craters not related to visible fractures are also found in the northern hemisphere, indicating there are subsurface

fracture systems which have weakened the crust in this area. Analyzing the d/D ratio for the four categories of PC across each latitude reveals a slightly lower value ratio (0.10 and 0.09 for the mean and oblate sphere models, respectively) than the average d/D found for the fresh craters on Ceres (0.11 and 0.10 for the mean and oblate sphere models, respectively). This indicates the craters do not have to excavate as far into the subsurface to encounter fracture systems that give rise to the polygonal shape.

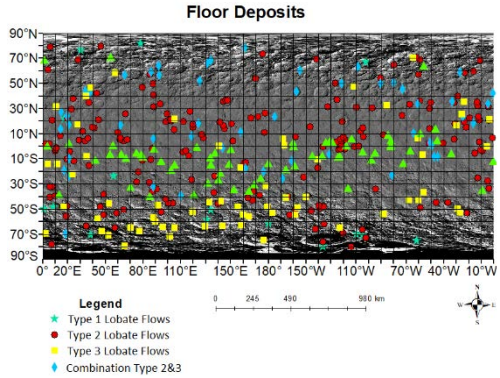

Figure 2: The distribution of the five types of lobate flow features found across Ceres.

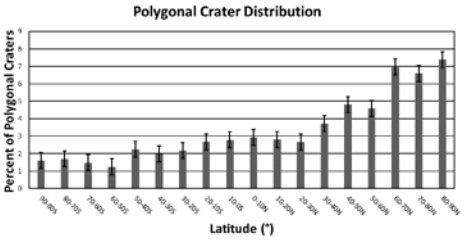

Figure 3: The percent of polygonal craters found across the surface of Ceres. Standard error bars were calculated.

Conclusions: These results suggest a hemispheric difference in crustal strength across Ceres. Central peaks, central pits, polygonal craters, and some lobate flows all suggest a weaker crustal strength in the northern hemisphere. These results indicate that Ceres has undergone some process (or multiple process) which have weakened the crust in the north. Crater size-frequency distribution analyses are being conducted to provide time constraints on when these changes occurred and provide insight into the origin(s) of the crustal weakening.

Acknowledgements: This research is supported by NASA PGG award NNX14AN27G to NGB.

References: [1] Park R. S. et al. (2016) *Nature* 537, 515-517. [2] Bland M. T. et al. (2013) *Icarus* 226,538-542. [3] Hesinger H. et al. (2016) *Science*, 353, aaf4759. [4] Barlow N. G. et al. (2017) *Meteoritics & Planetary Science* 52, 1371-1387. [5] Barlow N. G. and Tornabene L. L. (2018), *49th LPSC*, 1687. [6] Buczkowski D. L. et al. (2016), *Science*, 353, aaf4332. [7] Otto K. A. et al. (2016), 47th *LPSC*, 1493. [8] Neidhart T. et al. (2017), *48th LPSC*, 1625. [9] Gou S. et al. (2018) *Icarus*, 302, 296-307. [10] Zeilnhofer M. F. and Barlow N. G. (2019) 50th *LPSC*, 1259. [11] Öhman T. et al. (2008) *Meteoritics & Planetary Science*, 43, 1605-1628. [12] Zeilnhofer M. F. and Barlow N. G. (2018) *49th LPSC*, 1464. [13] Rotasch T. et al. (2017) *Planet. Space Sci*., 140, 74-79. [14] Gorelick, N. S., et al., (2003). *34th LPSC, 2057.*[15] Scully J. E. C. et al. (2017), *GRL*,44, 9564-9572. [16] Zeilnhofer M. F. and Barlow N. G. (2018) *9th PCC* 1801.